Computed circular polarization of line emissions for $\Delta n = 1$ transitions between highly excited states of hydrogenic ions in tokamak plasmas

L. K. Huang,* D. Wróblewski,† M. Finkenthal,‡ and H. W. Moos
Department of Physics and Astronomy, The Johns Hopkins University, Baltimore, Maryland 21218
(Received 21 April 1989)

Circular polarization of spectral lines due to $\Delta n = 1$ transitions between highly excited states ($n = 6-8$) of low-Z hydrogenic ions (C VI and O VIII) has been computed under tokamak plasma conditions. The numerical model includes relativistic corrections, the Zeeman effect, the motional Stark effect, and Doppler broadening. The motional Stark effect in spectral line profiles is negligible because of Doppler broadening. The Zeeman effect is described by the intensity-averaged splitting factor, which is equal to unity and independent of the Stark effect for all Rydberg lines (provided the n shells are well separated). The circular polarization of the line is proportional to the component of the magnetic field in the direction of the observation direction. An analytical expression for the polarization, as a function of the intensity-averaged Zeeman splitting and a characteristic linewidth, is formulated by fitting the numerical results obtained for a variety of plasma conditions and spectral lines.

I. INTRODUCTION

In a tokamak plasma, heating or probe neutral beams populate highly excited states of low-Z hydrogenic ions via charge-exchange recombination (CXR).[1,2] $\Delta n = 1$ transitions between the highly excited states have been observed in the visible and near-ultraviolet spectral ranges, e.g., O VIII 2976 Å ($n = 8 \rightarrow 7$), C VI 5291 Å ($n = 8 \rightarrow 7$), and C VI 3434 Å ($n = 7 \rightarrow 6$). These spectral lines have been used to measure ion temperature, plasma rotation velocity, and impurity density.[3-7] A possible application of these lines to measure the poloidal magnetic field in a tokamak was also suggested.[8] The measurement of the magnetic field is based on the analysis of the circular polarization of the line profiles, i.e., the analysis of the peak-to-peak value of the difference between the left-hand and the right-hand circularly polarized line profiles.[9] The circular polarization is proportional to the magnetic field component in the direction of observation. With the observation direction in the poloidal plane of a tokamak, the poloidal magnetic field can be measured. If a small-diameter diagnostic neutral beam is used, the CXR line emissions will be localized, enabling good spatial resolution of the measurement.

The ion temperature range in a tokamak plasma is 10^2-10^4 eV, and the external magnetic fields are 1–10 T. For the high-n states of the low-Z hydrogenic ions, the energy-level splitting due to both the Zeeman effect and the motional Stark effect (due to the Lorentz electric field seen by ions moving across the magnetic field, $\mathbf{E} \sim \mathbf{v} \times \mathbf{B}$) is comparable in magnitude to the fine-structure level splitting.[6] In general, the level splitting as a function of the external magnetic field is neither linear nor quadratic at such intermediate external field perturbation.[10] Severe level mixing is expected and the eigenstates of the ions cannot be approximated by pure LS coupled or uncoupled eigenstates. The mixing among different angular momentum eigenstates makes possible a large number of transitions forbidden by the selection rules, and many cancellations occur.[10] In order to use the CXR lines for diagnostic purposes, a rigorous analysis of the line profiles is needed. Particularly, the magnetic field measurement requires the knowledge of the shape of the circularly polarized line profiles, and of the line splitting as a function of the magnetic field. Many extensive studies of the CXR line profiles have been published.[1,2,6,7,11-14] However, rigorous computations of atomic structures of the low-Z hydrogenic ions in a tokamak environment were performed only for lower-n shells ($n = 3,4$).[12-14] This paper extends the computations to the high-n shells and determines the circular polarization of these lines for the magnetic field measurement.

Moreover, high-n shells possess rich fine structure, and there are hundreds of possible transitions between the highly excited states. Because of the Doppler broadening, the spectral components of the splitting due to the relativistic, Zeeman, and motional Stark effects are unresolvable. Thus it is more meaningful to work with quantities averaged over all levels and transitions, in contrast to the study of all individual transitions for the low-n shells.

In general, the CXR process selectively populates levels with different angular momentum quantum numbers;[1,2] thus the level population should be calculated by solving coronal equilibrium equations. However, since in the tokamak environment the collisional excitation and deexcitation rates within a high-n shell can be larger than the spontaneous decay rates, the level population in the n shell tends to be in statistical equilibrium.[6] For a typical tokamak plasma condition, $n_e = 2 \times 10^{13}$ cm^{-3}, $T = 1$ keV and $Z_{\text{eff}} = 2$, all levels with $n \geq 5$ for carbon and $n \geq 6$ for oxygen can be considered to be collisionally mixed.[6] Therefore a statistical level population within a shell considered is assumed in the present study.

The paper is organized as follows. Section II describes a numerical simulation of the line profiles originating from the $\Delta n=1$ transitions between highly excited states of low-Z hydrogenic ions in the tokamak plasmas, including the relativistic corrections, the Zeeman effect, and the motional Stark effect. Section III discusses the level mixing due to the Zeeman and the motional Stark effects. Section IV shows the Doppler broadening is dominant over the motional Stark effect. In Sec. V an intensity-weighted average splitting factor is analytically derived and compared with the numerically computed splitting between the peaks of the $\sigma_{\pm}$ line profiles. Section VI presents the circular polarization of line emissions described as a function of both the intensity-weighted Zeeman splitting and a characteristic linewidth for use in measurements of magnetic fields. The characteristic linewidth is described by an analytical function of the ion temperature and the magnetic field, determined by fitting the numerical results for the circular polarization.

II. COMPUTATION OF EIGENSTATES, EIGENENERGIES, TRANSITION PROBABILITIES, AND LINE PROFILES

An external uniform magnetic field in the z direction, Fig. 1, determines the axis of rotational symmetry. To avoid complex matrices in the computation, one can choose the ion velocity vector to be in the y direction. The Hamiltonian of the perturbation to the hydrogenic ion, including the relativistic correction, the Zeeman term, and the motional Stark term, is, in atomic units, given by

$$H_1=-\frac{\alpha^2}{4}(E_0-V)^2-\frac{\alpha^2}{4}\left[\frac{dV}{dr}\right]\frac{\partial}{\partial r}+\frac{\alpha^2}{2}\frac{1}{r}\left[\frac{dV}{dr}\right]\boldsymbol{l}\cdot\mathbf{s}$$
$$+\mu_0 B(l_z+g_s s_z)-2ex\left[\frac{v_y}{c}\right]B\ , \tag{1}$$

where $E_0=Z^2/n^2$ is the unperturbed eigenenergy, $V=-2Z/r$, B is the magnetic field strength, v_y is the velocity of the ion in the y direction, and the other symbols are conventional.[10]

A complete set of $2n^2$ wave functions for the n shell of the unperturbed hydrogenic ion, in either LS coupled or uncoupled representations, is used to construct the matrix of the perturbation Hamiltonian. Eigenvalues and eigenvectors of the real matrix are obtained with a double-precision computer code for diagonalization of a Hermitian matrix. [The computer code was revised from a single-precision code of the Centre Européenne pour la Recherche Nucléaire (CERN) program library.[15]] The fact that both the LS coupled and the LS uncoupled representations should result in the same eigenvalues and eigenvectors is used to check the correctness and the accuracy of the computation. The eigenvalues of the energy levels calculated in different representations match each other to within eight significant digits.

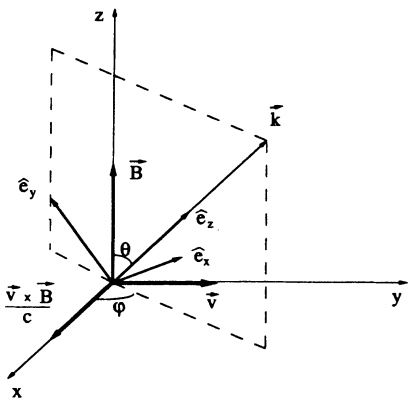

FIG. 1. Reference frame used in the numerical computations. The magnetic field is in the z direction. The ion moves in the y direction, and the Lorentz field is in the x direction. Emission is in an arbitrary direction of $\hat{\mathbf{e}}_z$. $(\hat{\mathbf{e}}_x,\hat{\mathbf{e}}_y,\hat{\mathbf{e}}_z)$ form a rectangular reference frame for the emission. $\hat{\mathbf{e}}_x=-\sin\phi\hat{\mathbf{x}}+\cos\phi\hat{\mathbf{y}}$, $\hat{\mathbf{e}}_y=-\cos\theta\cos\phi\hat{\mathbf{x}}-\cos\theta\sin\phi\hat{\mathbf{y}}+\sin\theta\hat{\mathbf{z}}$, and $\hat{\mathbf{e}}_z=\sin\theta\cos\phi\hat{\mathbf{x}}+\sin\theta\sin\phi\hat{\mathbf{y}}+\cos\theta\hat{\mathbf{z}}$. $r=(x^2+y^2+z^2)^{1/2}$.

To study the possible use of the CXR lines for the measurement of the tokamak poloidal magnetic field, the circularly polarized line profiles are computed. First, spontaneous decay rates as a function of emission direction are calculated. With the coordinate system in Fig. 1, the emission direction is $\hat{\mathbf{e}}_z$ with an angle of θ to the magnetic field vector $B\hat{\mathbf{z}}$; $\hat{\mathbf{e}}_x$, $\hat{\mathbf{e}}_y$, and $\hat{\mathbf{e}}_z$ form a Cartesian coordinate frame. The spontaneous decay rate for the circularly polarized emission in the direction $\hat{\mathbf{e}}_z$ is

$$A_{\pm}^{if}=a_{if}|\langle\Psi_i|\mathbf{r}\cdot\hat{\boldsymbol{\epsilon}}_{\pm}|\Psi_f\rangle|^2\ , \tag{2}$$

where $\hat{\boldsymbol{\epsilon}}_{\pm}=\mp(1/\sqrt{2})(\hat{\mathbf{e}}_x\pm i\hat{\mathbf{e}}_y)$, $\Psi_{i,f}$ are the eigenstates of the Hamiltonian of Eq. (1), i and f indicate the initial and final states of the transition, $a_{if}=4e^4a_0^2(E_i-E_f)^3/3\hbar^4c^3$, a_0 is the Bohr radius, and $E_{i,f}$ are the eigenenergies of the Hamiltonian. Using the laboratory coordinates for $\hat{\boldsymbol{\epsilon}}_{\pm}$, the decay rate can be rewritten as

$$A_{\pm}^{if}=\frac{a_{if}}{4}\{(1\mp\cos\theta)^2|\langle\Psi_i|r_-|\Psi_f\rangle|^2+(1\pm\cos\theta)^2|\langle\Psi_i|r_+|\Psi_f\rangle|^2$$
$$+2\sin^2\theta|\langle\Psi_i|r_0|\Psi_f\rangle|^2+2\cos(2\phi)\sin^2\theta\langle\Psi_i|r_-|\Psi_f\rangle\langle\Psi_i|r_+|\Psi_f\rangle$$
$$\pm2\sqrt{2}\cos\phi\sin\theta[(1-\cos\theta)\langle\Psi_i|r_-|\Psi_f\rangle+(1+\cos\theta)\langle\Psi_i|r_+|\Psi_f\rangle]\langle\Psi_i|R_0|\Psi_f\rangle\}\ , \tag{3}$$

where $r_{\pm}=\mp(1/\sqrt{2})(x\pm iy)$ and $r_0=z$. The correctness of numerical results for $\langle\Psi_i|r_q|\Psi_f\rangle$ $(q=\pm,0)$ was examined using the sum rules.[10]

In computing the broadening of the line profile, a Maxwellian velocity distribution is assumed. Because of the motional Stark effect, the wavelength in the reference frame associated with the emitting ion, as well as the transition

probability, is a function of the ion velocity. Thus the average over the ion's thermal motion includes both the Doppler effect and the motional Stark effect. Because the atomic data are azimuthally symmetric around the magnetic field direction, a rotation of the ion velocity around **B** is equivalent to a rotation of the emission direction around **B** with the ion moving in the fixed $\hat{\mathbf{y}}$ direction. The line profile of a single transition is given by

$$\overline{A}^{if}_{\pm}(\lambda,\theta)=\left[\frac{M}{2\pi kT}\right]^{3/2}\int_{-\infty}^{+\infty}dv_z\int_0^{\infty}v_r dv_r\int_0^{2\pi}d\phi\, A^{if}_{\pm}(v_r,\phi,\theta)e^{-M(v_r^2+v_z^2)/2kT}\delta(\lambda-\lambda_S)\ , \tag{4}$$

where k is the Boltzmann constant, T is the ion temperature, M is the ion mass, v_r is the velocity in the x-y plane (which is in y direction), v_z is the velocity in z direction, $\lambda_S=\lambda_{if}(1-\sin\theta\sin\phi\, v_r/c-\cos\theta\, v_z/c)$ is the Doppler-shifted wavelength, and $\lambda_{if}=hc/(E_f-E_i)$ is a function of v_r.

Because the atomic data are translationally invariant along the **B** field, a line profile observed in a reference frame in which the ion moves only perpendicular to **B** can be transformed to a line profile in the laboratory reference frame by using the Doppler broadening due to the thermal motion in the z direction only. Thus the integration in Eq. (4) can be done in two steps. The first step is an integration over the v_x-v_y plane with $v_z=0$,

$$\overline{A}^{if}_{p\pm}(\lambda,\theta)=\frac{M}{2\pi kT}\int_{v_{rm}}^{\infty}dv_r\frac{A^{if}_{\pm}(v_r,\cos\phi,\theta)+A^{if}_{\pm}(v_r,-\cos\phi,\theta)}{(\lambda_{if}/c)\sin\theta\cos\phi}e^{-Mv_r^2/2kT}\ , \tag{5}$$

where

$$\cos\phi=\left[1-\left[\frac{\lambda_{if}-\lambda}{\lambda_{if}}\right]^2\Big/\left[\frac{v_r\sin\theta}{c}\right]^2\right]^{1/2},$$

and v_{rm} is determined by

$$\frac{v_{rm}\sin\theta}{c}=\frac{\lambda_{if}(v_{rm})-\lambda}{\lambda_{if}(v_{rm})}\ .$$

In the second step, the $\overline{A}^{if}_{p\pm}$ profile is broadened due to the thermal motion only in the z direction,

$$\overline{A}^{if}_{\pm}(\lambda,\theta)=\int\frac{d\lambda'}{b\lambda'}\overline{A}^{if}_{p\pm}(\lambda',\theta)e^{-(\lambda-\lambda')^2/b^2\lambda'^2}\ , \tag{6}$$

where $b=(Mc^2/2kT\cos^2\theta)^{1/2}$. This two-step integration for the Doppler broadening is valid in the case of $v/c\ll 1$.

Finally, a statistical distribution for the level population is assumed, and the average is taken over all possible transitions,

$$\overline{A}_{\pm}(\lambda,\theta)=\frac{1}{2n^2}\sum_{i,f}\overline{A}^{if}_{\pm}(\lambda,\theta)\ , \tag{7}$$

where n is the principal quantum number of the upper level. According to Eq. (3), $\overline{A}_{\pm}$ at $\theta=0$ are reduced to spontaneous decay rates for the $\sigma_{\pm}$ transitions.[10]

In addition to the use of the different representations and the sum rules for examining the correctness of the computations, we calculated the line structures for the H I 6561-Å line (H_α) and the H I 4861-Å line (H_β), and compared our results with those obtained in Ref. 13 and 14. Our results agree with those of Breton *et al.* under all conditions, and agree with those of Souw and Uhlenbusch for the H_α line under two conditions [$B=5$ T and $v_r=2\times10^8$ cm/sec, Figs. 7(a) and 7(b) in Ref. 14]. However, their results under two other conditions [$B=5$ T, and $v_r=3\times10^7$ cm/sec and $v_r=4\times10^7$ cm/sec, respectively, Figs. 5(b) and 5(c) in Ref. 14] appear to be in error.

III. LEVEL MIXING

As expected, the computed eigenstates are far removed from the pure LS coupled states or the pure LS uncoupled states. As an example, the $n=8$ shell of the O VIII and the O VIII 2977-Å line at $T=1$ keV and $B=2.8$ T are discussed in the following.

The Zeeman effect can be isolated from the motional Stark effect at zero ion speed. In this case, l and m_j are good quantum numbers. It is observed in the computed results that states with $m_l\geq 4$ become LS uncoupled states. The Zeeman effect in the O VIII 2977-Å line at zero ion speed is demonstrated in Fig. 2(a), which shows the synthetic spectrum calculated as a sum of all individual components with a Gaussian linewidth of 0.01 Å. As shown in the figure, the Zeeman splitting broadens the fine-structure components and individual Zeeman components are unresolvable even at the very low temperature of 1000 K ($\sim$0.1 eV).

The synthetic spectrum is substantially changed when the Stark effect is included, as shown in Fig. 2(b) with the same condition as in Fig. 2(a) but $v_y=10^7$ cm/sec. At the high ion speed, the level mixing is strong. Individual eigenstates cannot be labeled by the eigen angular quantum numbers. However, each eigenstate can be traced back to a state (original state) at zero speed along smooth functions of both the eigenenergy and the eigenvector coefficients. In order to illustrate the level mixing due to the motional Stark effect, a standard deviation of the expectation values of l^2 from $l(l+1)$ is defined for a group of $(2l+1)$ eigenstates having the original states with the same l,

$$\sigma_l\equiv\left[\frac{\sum_i[\langle\Psi_i|l^2|\Psi_i\rangle-l(l+1)]^2}{2l+1}\right]^{1/2}. \tag{8}$$

The σ_l is a measure of the level mixing. It is plotted in Fig. 3(a) as a function of the ion speed. As expected, the larger l a group has, the lower speed is required to cause severe mixing. At $v_y=5.4\times10^7$ cm/sec, the values of σ_l

for different l groups are ordered in a way which can be qualitatively understood as follows. For a hypothetical state composed of all states in the n shell with equal weight, the expectation value of l^2 is $\frac{1}{2}(n^2-1)$. Larger motional Stark effect (associated with larger speed) tends to mix more different l states. Thus the expectation values of l^2 for the mixed states tend to approach $\frac{1}{2}(n^2-1)$. The σ_l values should be ordered according to (decreasing) magnitudes of $|l(l+1)-\frac{1}{2}(n^2-1)|$, which corresponds to $l=0,1,2,7,3,4,6,5$. This order is roughly followed in the example in Fig. 3(a) except for the groups of $l=0$ and 1, which have not been mixed with high-l states at $v_y=5.4\times10^7$ cm/sec because of their lower electrical dipole energy and larger energy gap.

To describe the level mixing in a whole n shell, we define $\bar{l}_i$ to be the expectation value of l: $\bar{l}_i(\bar{l}_i+1) \equiv \langle \Psi_i | l^2 | \Psi_i \rangle$. Then, the average standard deviation of $\bar{l}_i$ from the l_i of its original state, averaged over all of the eigenstates in the n shell, is defined as

$$\sigma_{\rm av} \equiv \left[\frac{\sum_i (\bar{l}_i - l_i)^2}{2n^2} \right]^{1/2} . \tag{9}$$

Figure 3(b) shows $\sigma_{\rm av}$ as a function of v_y. At $v_y=10^7$ cm/sec, the most probable speed of ions at 1 keV temperature, the average deviation is about 0.5. This indicates that the eigenstates mix with adjacent l states at about 1:1 ratio. For $v_y > 10^7$ cm/sec, the average deviation increases, but the increment becomes slower. This slowing-down tendency is due to the fact that, as the mixing among higher l states is extended to lower l states, the energy gaps between lower j states become increasingly larger,

$$\Delta E(\Delta j=1) = \frac{\alpha^2 Z^4}{n^3 (j+0.5)^2} , \tag{10}$$

while the electrical dipole energy in the Lorentz field is linearly proportional to the velocity. Thus the number of different l groups of orbital angular momentum eigenstates to be mixed in an eigenstate of Eq. (1) is a function of v_y^γ with $\gamma < 1$ for $v_y \geq 10^7$ cm/sec.

Note that the level mixing due to the motional Stark effect should be distinguished from the redistribution of

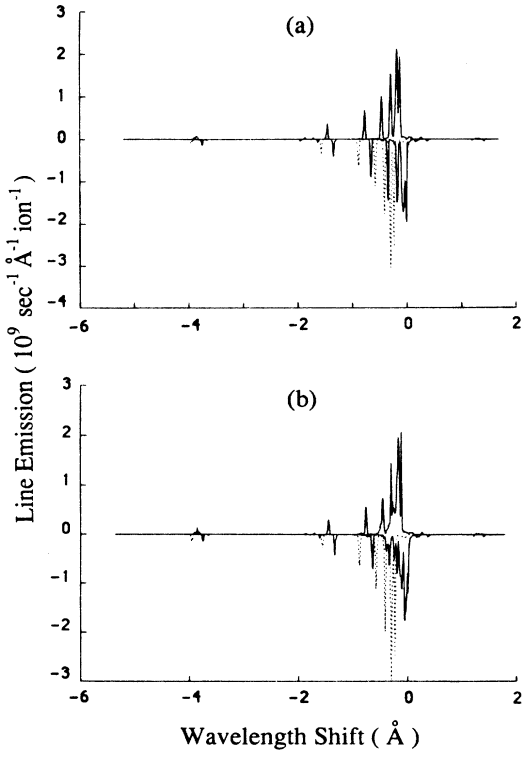

FIG. 2. Synthesized line profiles for O VIII 2977 Å at $B=2.8$ T. A Gaussian linewidth of 0.01 Å is assumed for each transition, which is equivalent to a Doppler broadening of the line at a temperature of 1000 K. The π components are drawn with positive values, and the $\sigma_\pm$ components are drawn with negative values. (a) The line profile for the ion at zero speed (no motional Stark effect). The fine-structure lines are broadened by the Zeeman effect. The Zeeman components are unresolvable. (b) The line profile for the ion at $v_y=10^7$ cm/sec. The motional Stark effect substantially changes the spectrum.

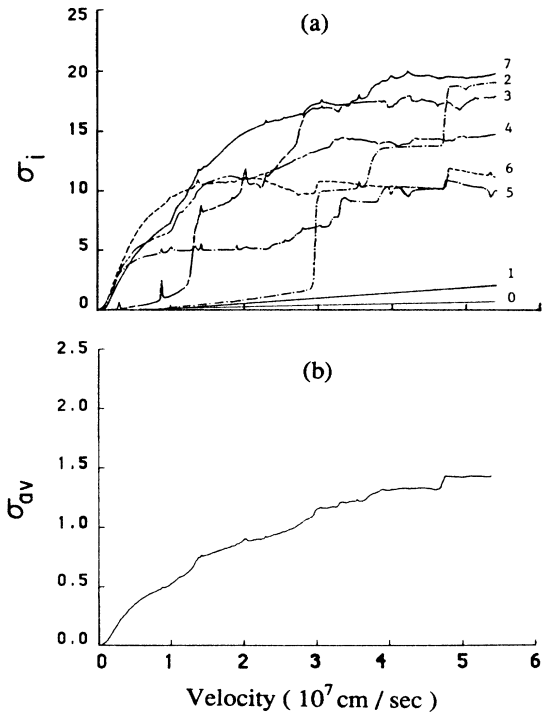

FIG. 3. (a) Standard deviation of the expectation values of l^2 (σ_i defined in Sec. III) as a function of ion speed perpendicular to the magnetic field for $n=8$ eigenstates of O VIII in a magnetic field of 2.8 T. The curves are labeled by the values of l for the original eigenstates at zero speed. (b) Standard deviation of the l quantum numbers averaged over all eigenstates ($\sigma_{\rm av}$ defined in Sec. III) as a function of the ion speed.

the CXR level population, which is also often called the level mixing.[6] As described above, the motional Stark effect mixes only the levels with adjacent l values. The CXR process is still expected to populate the levels selectively according to their different expectation values of angular momenta. Rigorous treatment of the effect on the collisional excitation and deexcitation within the n shell is beyond the scope of this work. A qualitative estimate is obtained by assuming that each l state may be coupled only with the adjacent $l\pm1$ states. A collision in the magnetic field may result in a transition from the initial l state to the final $l'\pm1$ states, whereas a similar collision in vacuum results only in the l' state. Therefore one may assume that the motional Stark effect results in the additional change of $\Delta l=1$ per collision. Then, at least $n-1$ consecutive collisions are needed before the radiative transition happens, for the motional Stark effect to be significant for the level population redistribution. However, the mean collision time in the plasma is found to be of the order of 10^{-5} sec,[16] which is much longer than the spontaneous decay time. Therefore the motional Stark effect does not change significantly the level population distribution and may be neglected in the estimate of the plasma parameters which result in the statistical level population.

IV. DOPPLER-BROADENING EFFECT

In the high-temperature plasma, the Doppler broadening is larger than the fine-structure splitting. The features of the line spectra due to the Zeeman splitting and the motional Stark effect are blended. Assuming a Doppler linewidth $\Delta\lambda_D$ larger than the whole fine-structure separation, as an example of extreme, the line profile can be approximated by

$$\sum_{i,f}\left(A_{\pm}^{if}e^{-(\lambda-\lambda_{if})^2/\Delta\lambda_D^2}\right)\simeq e^{-(\lambda-\lambda_{\pm})^2/\Delta\lambda_D^2}\left[\sum_{i,f}A_{\pm}^{if}\right], \quad (11)$$

where $\lambda_{\pm}$ are the peak wavelengths of the circularly polarized line profiles. As the sum of all transition probabilities is independent of the matrix representation, the profile is independent of the motional Stark effect. However, the computation shows that under the tokamak plasma conditions the polarized line profiles are approximately free of the motional Stark effect; including or excluding the motional Stark effect in the atomic data give approximately the same line profiles (the difference between the two is less than 10^{-4} of the peak) even at a temperature lower than that which enabled the approximation in Eq. (11).

As discussed in the preceding section, under the tokamak plasma conditions of $T=1$ keV and $B=2.8$ T, the Lorentz field mixes only the adjacent l states. A sum of transitions over the adjacent j states will be sufficient to eliminate the motional Stark effect. If the Doppler linewidth is broader than the wavelength separation between two adjacent lines of the fine structure, the line profile can be considered as free of the motional Stark effect. When the temperature increases, the Doppler linewidth increases linearly with v, faster than the increase of mixed number of l states. Therefore the ion temperature criterion to consider the line profile as Stark-effect–free can be determined from

$$\Delta\lambda_D=\lambda_0\left[\frac{2kT}{Mc^2}\right]^{1/2}>\lambda_0^2\frac{\alpha^2Z^4}{n^3(j+\frac{1}{2})^2}\frac{\mathrm{Ry}}{hc},$$

where $\mathrm{Ry}/hc=109\,737\ \mathrm{cm}^{-1}$ and $\lambda_0=hc/(E_{0i}-E_{0f})$ is the unperturbed wavelength in units of cm. Since the main concern here is the strongest transitions between high j states, the $j+\frac{1}{2}$ in the above equation may be replaced by $n/2$. For O VIII 2977-Å line, the criterion gives $kT>56$ eV. Since the actual temperature is 1 keV, much higher than the criterion, the motional Stark effect is indeed negligible. As a qualitative estimate, assuming the Doppler broadening be larger than the line splitting of the motional Stark effect, one can find the following condition for neglecting the motional Stark effect:

$$3.2\times10^{-7}\frac{n^4(n-1)^2B}{(2n-1)Z^3}\le1, \quad (12)$$

where B is in G, n is the principal quantum number for the upper levels. From Eq. (12), the O VIII 2977-Å line profile can be approximately free of the motional Stark effect in a magnetic field of up to 10 T, which is also confirmed by the results of the exact computation.

V. INTENSITY-WEIGHTED AVERAGE SPLITTING FACTOR

As shown in the preceding section, individual components of $\Delta n=1$ transitions between highly excited states of low-Z hydrogenic ions in a tokamak plasma are unresolvable, and the measured line profile is an average over hundreds of transitions. It is convenient to introduce an average line splitting weighted by the spontaneous decay rate,

$$\Delta\bar{\lambda}_B=\frac{1}{2}\left[\frac{\sum_{i,f}a_{if}|\langle\Psi_i|r_+|\Psi_f\rangle|^2\lambda_{if}}{\sum_{i,f}a_{if}|\langle\Psi_i|r_+|\Psi_f\rangle|^2}-\frac{\sum_{i,f}a_{if}|\langle\Psi_i|r_-|\Psi_f\rangle|^2\lambda_{if}}{\sum_{i,f}a_{if}|\langle\Psi_i|r_-|\Psi_f\rangle|^2}\right], \quad (13)$$

where the summation is over all states in the initial and the final shells. $2\Delta\bar{\lambda}_B$ is the splitting between the σ_- and σ_+ line peaks. In the case where the energy-level splitting in a shell is much smaller than the energy separation between different n shells, Eq. (13) can be approximated [to an accuracy of $(\Delta E_i-\Delta E_f)/(E_i-E_f)$] by

$$\Delta\bar{\lambda}_B=\frac{\lambda_0^2}{2hcA}\left[\sum_{i,f}|\langle\Psi_i|r_+|\Psi_f\rangle|^2(\Delta E_f-\Delta E_i)-\sum_{i,f}|\langle\Psi_i|r_-|\Psi_f\rangle|^2(\Delta E_f-\Delta E_i)\right], \tag{14}$$

where ΔE_i and ΔE_f are the level shifts of the initial and the final states, and

$$A=\sum_{i,f}|\langle\Psi_i|r_+|\Psi_f\rangle|^2=\sum_{i,f}|\Psi_i|r_-|\Psi_f\rangle|^2 .$$

$(\Delta E_f-\Delta E_i)$ in Eq. (14) can be rewritten as matrix elements of the $[H_1,r_\pm]$ commutators,

$$\Delta\bar{\lambda}_B=\frac{\lambda_0^2}{2hcA}\left[\sum_{i,f}\langle\Psi_i|[H_1,r_+]|\Psi_f\rangle\langle\Psi_f|-r_-|\Psi_i\rangle-\sum_{i,f}\langle\Psi_i|[H_1,r_-]|\Psi_f\rangle\langle\Psi_f|-r_+|\Psi_i\rangle\right] . \tag{15}$$

Because the coupling between different n shells is negligible in our case, the summations in Eq. (15) are invariant with respect to any unitary transformation of the representation. One can arbitrarily choose a representation of pure LS coupled or LS uncoupled states for Eq. (15). As the motional Stark term in the H_1 commutes with $r_\pm$, it can be dropped from the commutators in Eq. (15). Thus $\Delta\bar{\lambda}_B$ is independent of the motional Stark effect. Although the electrical dipole energy of the ion in an external electric field is not included in Eq. (1), the Stark term (also commuting with r_q) will not affect $\Delta\bar{\lambda}_B$, either. Further, the relativistic part of H_1 can be dropped. Indeed, by choosing a representation of pure LS coupled states, the relativistic part of the Hamiltonian produces the same fine structures for both σ_+ and σ_- lines, which then cancel each other in Eq. (15). The commutator of the spin operator in the Zeeman term with $r_\pm$ is zero. Finally, only $\mu_0 Bl_z$ of the Zeeman term is left in the commutators in Eq. (15). Choosing a representation of LS uncoupled pure states, $|n\rangle$, one obtains

$$\Delta\bar{\lambda}_B=\frac{\lambda_0^2}{2hc}\left[\frac{\sum_{i,f}\langle n_i|[\mu_0 Bl_z,r_+]|n_f\rangle\langle n_f|-r_-|n_i\rangle}{\sum_{if}|\langle n_i|r_+|n_f\rangle|^2}-\frac{\sum_{if}\langle n_i|[\mu_0 Bl_z,r_-]|n_f\rangle\langle n_f|-r_+|n_i\rangle}{\sum_{if}|\langle n_i|r_-|n_f\rangle|^2}\right]=\frac{\mu_0\lambda_0^2 B}{2\pi\hbar c} . \tag{16}$$

One may define an intensity-weighted average splitting factor $\bar{z}$ by

$$\Delta\bar{\lambda}_B=\bar{z}\frac{\mu_0\lambda_0^2 B}{2\pi\hbar c} . \tag{17}$$

A comparison of Eq. (17) with Eq. (16) gives $\bar{z}=1$ for all Rydberg series. This result is generally valid, regardless of the relativistic corrections and any type of Stark effect, provided different n shells are well separated in energy.

The above result is important for the magnetic field measurement. It ensures a linear relation between the Zeeman splitting and the magnetic field, therefore a linear relation between the measured polarization signal and the magnetic field in the observation direction regardless of the complicated level mixing.

Note that the above definition for $\Delta\bar{\lambda}_B$ corresponds to the measurement of the peak separation between the σ_- and the σ_+ lines in a high-temperature plasma. The use of a Zeeman triplet model, π and $\sigma_\pm$, to describe the Zeeman splitting of the complicated fine structure is valid only in a high-temperature plasma where the fine structure of the lines is blended. Figure 4 shows good agreement between $\Delta\bar{\lambda}_B$ and the splitting (divided by 2) between peaks of the σ_+ and σ_- line profiles obtained numerically for different ion temperatures as a function of magnetic field.

VI. CIRCULAR POLARIZATION AND APPLICATION TO THE MAGNETIC FIELD MEASUREMENT

For the magnetic field measurement, a directly measurable quantity is[17]

$$\rho(\lambda)=\frac{I_+(\lambda)-I_-(\lambda)}{I_+(\lambda_0)+I_-(\lambda_0)} , \tag{18}$$

where I_+ and I_- are the right-hand and the left-hand circularly polarized line intensity profiles, λ is the wavelength and λ_0 is the central wavelength of the line profile. One of the computed $\rho(\lambda)$ profiles is shown in Fig. 5. Ac-

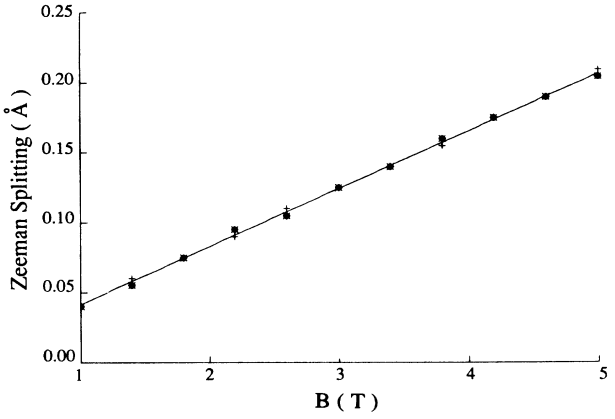

FIG. 4. Comparison of the Zeeman splitting between the analytically derived $\Delta\bar{\lambda}_B$ (the intensity-weighted average splitting) and the numerically computed peak separation (divided by 2) between the $\sigma_\pm$ line profiles ($\Delta\lambda_B$) the for O VIII 2977-Å line in tokamak plasma. The solid line is $\Delta\lambda_B$. The discrete data points are the numerical results at ion temperatures of 0.1 (+), 0.5 (*), 1.0 (●), and 1.5 (◇) keV.

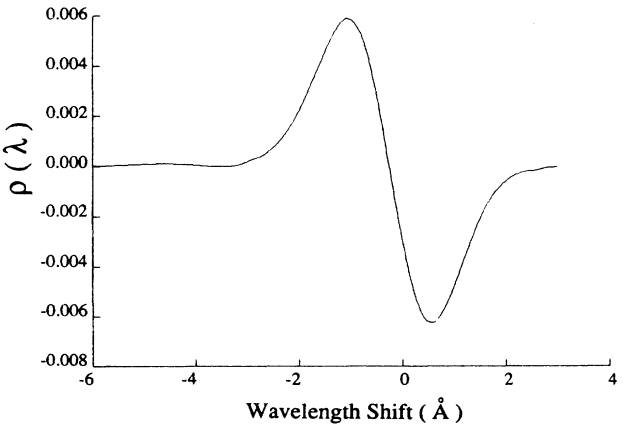

FIG. 5. Difference between the left-hand and the right-hand circularly polarized line profiles, $\rho(\lambda)$, for the O VIII 2976 Å with $B=28$ kG, $T=1$ keV, and $B\cos\theta=1.98$ kG.

cording to Eq. (3), $\rho(\lambda)$ is proportional to the product of $\cos\theta$ and the difference between the σ_+ and σ_- line profiles. As the Zeeman splitting is small compared to the width of the line profiles, the peak-to-peak value of $\rho(\lambda)$, a measure of the circular polarization of the spectral line, can be approximated by

$$\Delta\rho\equiv\rho_{\max}-\rho_{\min}\simeq\frac{4\cos\theta\Delta\bar{\lambda}_B}{\sqrt{2e}\,\Delta\lambda_D^*}\ , \tag{19}$$

where the numerical coefficient is determined assuming the Gaussian line profiles, and $\Delta\lambda_D^*$ is the characteristic linewidth [the half-width at $1/e$ of $I_\pm(\lambda)$ for the $\sigma_\pm$ lines]. If the line profile is Gaussian and the Doppler broadening is the sole broadening mechanism, $\Delta\lambda_D^*=\Delta\lambda_D=\lambda_0(2kT/mc^2)^{1/2}$. In general, the line profiles are not Gaussian, and $\Delta\rho$ depends on the shape of the line profiles.

In order to express the numerically computed $\Delta\rho$ in a convenient form, the characteristic linewidth $\Delta\lambda_D^*$ is computed by using Eq. (19) and the numerically computed $\Delta\rho$. The numerical results for $\Delta\lambda_D^*$ are then fitted with a suitable function. The fitting function is chosen assuming that the line profile is dominated by the Doppler broadening, with the primary correction due to the fine-structure splitting,

$$\Delta\lambda_D^*=\left[\Delta\lambda_D^2+\left[\frac{4\alpha^2Z^4\lambda^2}{n^5}\frac{\mathrm{Ry}}{hc}\Delta j\right]^2\right]^{1/2}\ , \tag{20}$$

where the wavelength is in cm and $\mathrm{Ry}/hc=109\,739$ cm^{-1}. The second term within the square brackets in Eq. (20) is taken from Eq. (10) with $j+0.5=n/2$ and an arbitrary Δj,

$$\Delta j=a_0+a_1B+1.5T^{0.25}\ , \tag{21}$$

where B is the magnetic field in tesla, T is the ion temperature in keV, and the numbers associated with T are chosen for the best fitting of Δj to the numerical result of $\Delta\rho$ with a broad range of the plasma conditions for different lines. a_0 and a_1 in Eq. (21) are also the fitting parameters and they are listed in Table I for O VIII 2976-Å, C VI 5292-Å, and C VI 3434-Å lines. The term of a_1B may be related to the Zeeman effect and is small. The slowly varying term of the temperature, $1.5T^{0.25}$, dominates Δj, and becomes less important compared to $\Delta\lambda_D$ at high temperature. $a_0+1.5T^{0.25}$ provides the basic correction for the fine structure. Note that the motional Stark term should be in the form of $B\sqrt{T}$, and that the temperature-dependent term in Δj is, therefore, not directly associated with the motional Stark effect. Although $\Delta\lambda_D^*$ involves B, the nonlinearity of $\Delta\rho$ on B is extremely small and negligible. With Eqs. (17), (19)–(21), and Table I, the $\Delta\rho$ can be calculated for various plasma conditions.

TABLE I. Coefficients of Eq. (17) and circular polarization. $\Delta\rho$ is given at $T=1$ keV, $B=2.8$ T, and $B\cos\theta=0.198$ T.

Lines	O VIII 2976 Å	C VI 5292 Å	C VI 3424 Å
a_0	0.01	0.274	0.317
a_1	0.024	0.177	0.050
$\Delta\rho$	0.0121	0.0192	0.0124

Table I also lists a few sample values of $\Delta\rho$. At the line brightness level of $10^{11}-10^{12}$ photon/cm^2 sr sec, $\Delta\rho$ of the order of 10^{-3} can be measured in a tokamak plasma. Therefore, at the listed tokamak conditions, which are typical for a medium size tokamak such as the Texas Experimental Tokamak,[18] the CXR lines are suitable spectral sources for the magnetic field measurement with an accuracy of the order of 0.01 T. The magnitude of $\Delta\rho$ is roughly proportional to $B/\sqrt{T}$. This scaling can be obtained by substituting Eqs. (17) and (20) into Eq. (19) for $\Delta\bar{\lambda}_B$ and $\Delta\lambda_D^*$, with an approximation that the linewidth is dominated by the Doppler broadening. In large size tokamaks, the ion temperature may be much higher than 1 keV and the Doppler broadening is indeed dominant; as the magnetic field also tends to be larger, the ratio of $B/\sqrt{T}$, and therefore $\Delta\rho$, should be of the same order of magnitude for the both medium and large size tokamaks. Advantages of using the CXR lines of a diagnostic neutral beam are that the spectral source for the measurement can be localized and can be observed in high-density plasmas;[3–7] while other magnetic field diagnostics are either nonlocal or limited to low-density plasmas.[17,19,20]

VII. CONCLUSIONS

It appears that the circular polarization of the charge-exchange recombination lines of $\Delta n=1$ transitions of the low-Z hydrogenic ions may be employed for the magnetic field measurements in magnetically confined plasmas. The circularly polarized line emission profiles in a high-temperature plasma are free of the Stark effect. The intensity-averaged Zeeman splitting factor is unity. The circular polarization is, to high accuracy, a linear function of the magnetic field component in the observation direction.

ACKNOWLEDGMENTS

This work was supported by U.S. Department of Energy Grant No. DE-FG02-85ER-53214-A000.

*Present address: Fusion Research Center, University of Texas, Austin, TX 78712.
†Present address: Lawrence Livermore National Laboratory, University of California, Livermore, CA 94550.
‡On sabbatical leave from Racah Institute of Physics, The Hebrew University, Jerusalem.

[1]R. E. Olson, Phys. Rev. A **24**, 1726 (1981).
[2]W. Fritsch and C. D. Lin, Phys. Rev. A **29**, 3039 (1984).
[3]R. J. Fonck, M. Finkenthal, R. J. Goldston, D. L. Herndon, R. Hulse, and D. D. Meyerhofer, Phys. Rev. Lett. **49**, 737 (1982).
[4]R. J. Groebner, N. H. Brooks, K. H. Burrell, and L. Rottler, Appl. Phys. Lett. **43**, 920 (1983).
[5]S. Suckewer, C. H. Skinner, B. Stratton, R. Bell, A. Cavallo, J. Hosea, D. Hwang, and G. Schilling, Appl. Phys. Lett. **45**(3), 236 (1984).
[6]R. J. Fonck, D. S. Darrow, and K. P. Jaehnig, Phys. Rev. A **29**, 3288 (1984).
[7]R. C. Isler, Phys. Scr. **35**, 650 (1986).
[8]D. Wroblewski and H. W. Moos, Rev. Sci. Instrum. **57**, 2029 (1986).
[9]U. Feldman, J. F. Seely, N. R. Sheely, S. Suckewer, and A. M. Title, J. Appl. Phys. **56**, 2512 (1985).
[10]R. D. Cowan, *The Theory of Atomic Structure and Spectra* (University of California Press, Berkeley, 1981).
[11]D. H. Sampson, J. Phys. B **10**, 749 (1979).
[12]R. C. Isler, Phys. Rev. A **14**, 1015 (1976).
[13]C. Breton, C. DeMichelis, M. Finkenthal, and M. Mattioli, J. Phys. B **13**, 1703 (1980).
[14]E. K. Souw and J. Uhlenbusch, Physica **122C** (1983).
[15]J. M. Boyle, S. G. Burton, and B. T. Smith, Program Library Long Write-up, CERN Computer Center Report No. F220, 1974 (unpublished).
[16]B. A. Trubnikov, in *Reviews of Plasma Physics,* edited by A. M. A. Leontovich (Consultants Bureau, New York, 1965), Vol. 1, p. 105.
[17]D. Wroblewski, L. K. Huang, and H. M. Moos, Rev. Sci. Instrum. **59**, 2341 (1988).
[18]K. W. Gentle, Nucl. Technol. Fusion **1**, 479 (1981).
[19]H. Soltwisch, Rev. Sci. Instrum. **57**, 1939 (1986).
[20]W. P. West, D. M. Thomas, J. S. deGrassie, and S. B. Zheng, Phys. Rev. Lett. **58**, 2758 (1987).